

Vac7p, a Novel Vacuolar Protein, Is Required for Normal Vacuole Inheritance and Morphology

CECILIA J. BONANGELINO, NATALIE L. CATLETT, AND LOIS S. WEISMAN*

Department of Biochemistry, University of Iowa, Iowa City, Iowa 52242

Received 25 June 1997/Returned for modification 5 August 1997/Accepted 17 September 1997

During cell division, the vacuole of *Saccharomyces cerevisiae* partitions between mother and daughter cells. A portion of the parental vacuole membrane moves into the bud, and ultimately membrane scission divides the vacuole into two separate structures. Here we characterize two yeast mutations causing defects in vacuole membrane scission, *vac7-1* and *vac14-1*. A third mutant, a *fab1-2* strain, isolated in a nonrelated screen (A. Yamamoto et al., *Mol. Biol. Cell* 6:525–539, 1995) shares the vacuolar phenotypes of the *vac7-1* and *vac14-1* strains. Unlike the wild type, mutant vacuoles are not multilobed structures; in many cases, a single vacuole spans both the mother and bud, with a distinct gap in the mother-bud neck. Thus, even where the membranes are closely opposed, vacuole fission is arrested. Simply enlarging the vacuole does not produce this mutant phenotype. An additional common phenotype of these mutants is a defect in vacuole acidification; however, vacuole scission in most other vacuole acidification mutants is normal. An alteration in vacuole membrane lipids could account for both the vacuole membrane scission and acidification defects. Because a directed screen has not identified additional class III complementation groups, it is likely that all three genes are involved in a similar process. Interestingly, *FAB1* was previously shown to encode a putative phosphatidylinositol-4-phosphate 5-kinase. Moreover, overexpression of *FAB1* suppresses the *vac14-1* mutation, which suggests that *VAC14* and *FAB1* act at a common step. *VAC7* encodes a novel 128-kDa protein that is localized at the vacuole membrane. This location of Vac7p is consistent with its involvement in vacuole morphology and inheritance.

Vesicle formation is an integral part of many cellular processes, including secretion, endocytosis, protein sorting, and maintenance of organelle identity (28, 34). When a vesicle buds, proteins and other cargo to be transported are concentrated at the site selected for the future vesicle, the membrane is deformed, and finally membrane scission releases the vesicle from the parent membrane. The newly formed vesicles travel to a target membrane, where they fuse and release their cargo.

Recently, proteins involved in homotypic membrane fusion have been identified for several cellular organelles. Sec18p (NSF) and Sec17p (α -SNAP), which are required for heterotypic fusion throughout the secretory pathway, are also required for homotypic fusion of the vacuole (17, 55) and for reassembly of the Golgi stacks (30). Molecules with homology to NSF have also previously been implicated in homotypic fusion events, such as the ATPase, Cdc48p, for yeast endoplasmic reticulum fusion (26) and its mammalian homolog, p97, in Golgi stack formation (1, 30). Membrane scission is a specialized form of homotypic membrane fusion. However, for scission, fusion initiates at the internal faces of the membranes, not the cytoplasmic faces. Thus, some constraints and requirements of scission most likely differ from the homotypic fusion described above, whereas the molecular basis for fusion of the phospholipid bilayer may be similar.

Dynamin is a GTPase required for scission of clathrin-coated endocytic vesicles. A mutant form of dynamin in shibire neuronal cells gives rise to tubular membrane invaginations that are visible by electron microscopy (24); similar structures are seen when synaptosomes are treated with GTP γ S (44). These membrane invaginations are endocytic vesicles that re-

main connected to the membrane because the scission event is blocked by inactive dynamin (10). These findings demonstrate that membrane scission is enzyme catalyzed. Moreover, they suggest that all types of membrane traffic, whether clathrin dependent or independent, require a specific mechanism for membrane scission. However, the *Saccharomyces cerevisiae* genome encodes only three dynamin homologs, Dnm1p, which is involved in endocytosis (12); Vps1p, which acts in the formation of Golgi vesicles destined for the vacuole (33) (reviewed in reference 8); and Mgm1p, which is implicated in proper division of the mitochondrial genome (16, 20). Thus, other molecules must catalyze the scission of vesicles formed from other organelles.

The process of membrane scission involves at least two events. First, the opposing luminal membranes must be brought into close proximity; second, the membranes must fuse to produce two distinct entities, the vesicle and the parent membrane organelle. It is likely that both proteins and phospholipids play equally important roles in membrane scission. For instance, proteins may play a critical role in bringing the membranes close together, similar to docking in heterotypic fusion events, or in catalyzing the fission of the membrane, similar to the role of dynamin. In contrast, the phospholipid composition of the membrane determines membrane flexibility and thus the ability of that section of membrane to obtain an appropriate shape and bend to form vesicles of the proper size. Additionally, a localized change in phospholipid composition may accompany or catalyze fusion.

Vacuole inheritance in *S. cerevisiae* is a form of membrane traffic. During cell division, the mother vacuole donates vacuole membranes and their luminal contents to the daughter cell (50–52). This occurs through the formation of a tubular or vesicular segregation structure that buds from the mother vacuole. The process is both spatially regulated and coordinated

* Corresponding author. Mailing address: Department of Biochemistry, University of Iowa, Iowa City, IA 52242. Phone: (319) 335-8581. Fax: (319) 335-9570. E-mail: lois-weisman@uiowa.edu.

TABLE 1. Strains used in this study

Strain	Genotype(s)	Reference
RHY6210	<i>MATα leu2,3-112 ura3-52 his3-Δ200 trp1-Δ901 lys2-801 suc2-Δ9 pep4-Δ1137</i>	15
JBY007	RHY6210 <i>vac7-1</i>	15
LWY7217	<i>MATα leu2,3-112 ura3-52 his3-Δ200 trp1-Δ901 lys2-801 suc2-Δ9</i>	This study
LWY2806	<i>MATα leu2,3-112 ura3-52 his3-Δ200 trp1-Δ901 lys2-801 suc2-Δ9 vac7-1 ade8Δ::HIS3</i>	This study
EMY119	<i>MATα leu2,3-112 ura3-52 his3-Δ200 trp1-Δ901 lys2-801 suc2-Δ9 fab1-2</i>	56
LWY6212	<i>MATα/a leu2,3-112 ura3-52 his3-Δ200 trp1-Δ901 lys2-801 suc2-Δ9 ade2::URA3</i>	This study
LWY1481	LWY6212 <i>vac7Δ::HIS3</i>	This study
LWY1527	<i>MATα leu2,3-112 ura3-52 his3-Δ200 trp1-Δ901 lys2-801 suc2-Δ9 vac7Δ::HIS3</i>	This study
LWY2365	LWY7217 <i>vac14-1</i>	This study
LWY7231	<i>MATα leu2,3-112 ura3-52 his3-Δ200 trp1-Δ901 lys2-801 suc2-Δ9 ade8Δ::HIS3</i>	This study
LWY7235	<i>MATα leu2,3-112 ura3-52 his3-Δ200 trp1-Δ901 lys2-801 suc2-Δ9</i>	This study
JK9-3D	<i>MATα leu2,3-112 ura3-52 trp1-1 his4 rme1 HMLα</i>	18a
LWY3467	RHY6210 with pCB26 (three-HA-tagged <i>VAC7</i> CEN)	This study
LWY3468	RHY6210 with pCB27 (six-HA-tagged <i>VAC7</i> CEN)	This study
LWY3469	RHY6210 with pCB28 (12-HA-tagged <i>VAC7</i> CEN)	This study
LWY3470	LWY1527 with pCB26	This study
LWY3471	LWY1527 with pCB27	This study
LWY3472	LWY1527 with pCB28	This study
LWY3849	LWY2365 with pNC2 (pRS416-FAB1)	This study
LWY3850	LWY2365 with pEMY105 (<i>FAB1</i> 2 μ m) (56)	This study
LWY2614	<i>MATα leu2,3-112 ura3-52 his3-Δ200 trp1-Δ901 lys2-801 suc2-Δ9 fab1-2 vac14-1</i>	This study
LWY2310	<i>MATα leu2,3-112 ura3-52 his3-Δ200 trp1-Δ901 lys2-801 suc2-Δ9 fab1-2 vac7-1</i>	This study
LWY4679	<i>MATα leu2,3-112 ura3-52 his3-Δ200 trp1-Δ901 lys2-801 suc2-Δ9 vac7-1 vac14-1</i>	This study

with the cell cycle (14, 53). Recent evidence suggests that vacuole segregation requires actin, Myo2p, and other cytoskeletal components (19). As with vesicle formation, the formation of the daughter vacuole is not complete until membrane scission releases it from the parent membrane. In addition to its importance for vacuole inheritance, membrane scission has a role in determining vacuole morphology. In wild-type yeast cells, the vacuole is usually multilobed; it is likely that membrane scission is involved in the formation and maintenance of these lobes.

Several vacuole inheritance mutants, isolated through selection with a fluorescence-activated cell sorter, were previously divided into three classes based on vacuole morphology (49). Among these, class III mutants contain enlarged, unlobed vacuoles that can occupy nearly the entire cytoplasm of the cell. Two class III mutants, *vac7* (15) and *vac14* strains, were identified due to a defect in vacuole inheritance. A third mutant, a *fab1-2* strain, was identified in an unrelated screen (56). Cells of these mutant strains contains an enlarged, unlobed vacuole and during cell division exhibits the characteristic open figure eight vacuole morphology and a segregation defect. As we describe here, vacuole membrane scission in these mutants is greatly impaired. Because even wild-type vacuoles are relatively large, this new class of mutants provides a means for studying membrane scission by fluorescence microscopy, whereas a scission defect in vesicles is difficult to visualize and, even in the best cases, has been detected only by electron microscopy (24, 45). We report the characterization of these class III mutants and demonstrate that their vacuolar phenotypes are not indirect effects due to the sizes of their vacuoles. In addition, the identification and localization of Vac7p, a protein required for membrane scission, are described. Vac7p localizes to the vacuolar membrane, which places it at the proper location to be directly involved in vacuolar membrane scission.

MATERIALS AND METHODS

Media, strains, and molecular biology techniques. Yeast extract-peptone-dextrose (YEPD) medium, synthetic complete medium, synthetic medium with

out uracil, and sporulation medium were made as previously described (21). High-pH YEPD plates with 1.6 M ethylene glycol were made as follows: 1% yeast extract, 2% Bacto Peptone, and 1.5% agar were autoclaved in 600 ml of water, and 50 ml of sterile 40% dextrose, 200 ml of sterile 7.5 M ethylene glycol, and 100 ml of 1 M potassium phosphate (pH 7.6) were added to the sterile YEP base. High-NaCl plates were standard YEPD plates supplemented with 1.5 M NaCl, and high-KCl plates were YEPD plates supplemented with 1.0 M KCl. The strains used in this study are listed in Table 1.

Diploid cells were sporulated, and tetrads were dissected as previously described (21). Yeast cells were transformed by the lithium acetate method (13). DNA manipulations and transformations into competent *Escherichia coli* DH5 α cells were performed by standard protocols.

Labeling yeast vacuoles with FM4-64. To visualize yeast vacuoles in vivo, log-phase cells were labeled with *N*-(3-triethylammoniumpropyl)-4-(*p*-diethylaminophenyl)hexatrienyl (FM4-64) as previously described (48) with a few modifications. Cells were incubated in medium containing 80 μ M FM4-64 (Molecular Probes, Eugene, Oreg.) for 1 h with shaking at 24°C. For synthetic medium, PIPES [piperazine-*N,N'*-bis(2-ethanesulfonic acid); pH 6.8] was added to a final concentration of 20 mM prior to the addition of FM4-64. Cells were washed three times with fresh medium, resuspended in 5 ml of fresh medium, and allowed to double (3 to 4 h) with shaking at 24°C. One milliliter of culture was harvested at 1,070 \times g for 3 min and viewed with a Pan-Neofluor 100 \times objective lens on a Zeiss Axioskop fluorescence microscope (excitation, 546 nm; emission, 580 to 630 nm). Photographs were taken with an attached 35-mm camera and Kodak TMAX400 film and developed according to the manufacturer's instructions for an ASA of 1,600.

To monitor vacuole inheritance and morphology in yeast zygotes (49, 53, 54), labeled haploid strains were washed as described above and placed into 5 ml of fresh YEPD medium. Labeled cells were incubated at 24°C for 1 h, and then an equal number of unlabeled cells of the opposite mating type was added. Cells were shaken at 24°C and allowed to mate for 4 to 4.5 h. Zygotes with medium-to-large buds were scored for the presence of FM4-64 in buds and originally unlabeled parents. The vacuole morphology in all cells was also scored.

Chemical additions to swell vacuoles. To swell vacuoles by the addition of imidazole, cells were grown overnight at 30°C in YEPD medium buffered with 50 mM potassium phosphate (pH 7.6). Imidazole (99%; Sigma) was added to a final concentration of 10 mM, and incubation was continued at 30°C for 3 h. Cells were labeled with FM4-64 and photographed.

To swell vacuoles by the addition of rapamycin, cells were grown in YEPD medium overnight at 30°C. Rapamycin (Drug Synthesis and Chemistry Branch, Developmental Therapeutic Program, Division of Cancer Treatment, National Cancer Institute) was added to a final concentration of 0.8 μ g/ml, and incubation was continued at 30°C for 3 h. YEPD medium was buffered with 20 mM PIPES (pH 6.8) during labeling with FM4-64. Cells were examined after a chase period of one doubling.

Measurement of vacuole size. Vacuoles were measured from images of FM4-64-labeled cells that were magnified 1,800-fold. The diameters of vacuoles in both unbudded and budded cells were scored. For budded cells, only the vacuoles of mother cells were scored. Measurements from 8- by 10-inch photographs

were calibrated with a microscope micrometer scale. Mean diameters and standard deviations (70% confidence level) were calculated from ≥ 75 cells (unless otherwise stated), assuming a Gaussian distribution of vacuole sizes.

Quinacrine labeling. Quinacrine labeling of log-phase cells was performed as previously described (51). One milliliter of yeast cells in log phase was harvested, resuspended in 500 μ l of 200 μ M quinacrine in phosphate-buffered YEPD medium (pH 7.6), and incubated for 5 min at room temperature. Cells were washed twice in fresh medium and viewed by fluorescence microscopy. Fluorescence (excitation, 450 to 490 nm; emission, ≥ 520 nm) was combined with a low level of transmitted light to reveal cell outlines.

DNA sequencing of *VAC7*. The *VAC7* clone was sequenced partially by PCR sequencing (36) and partially with a Sequenase 2.0 sequencing kit (Amersham Life Science). The open reading frame was fully sequenced on both strands.

Construction of a strain with *LEU2* integrated at the *VAC7* locus and deletion of *VAC7*. To construct a *LEU2-VAC7*-marked strain, a 1.6-kb *SacI-SacI* fragment that overlapped with the *VAC7* open reading frame was subcloned into pRS305 (37). This plasmid was linearized with *NruI*, which cuts in the center of the insert, and transformed into wild-type yeast strain LWY7217. PCR with genomic DNA isolated from the transformed strain (9) was done to ensure that proper integrants were obtained. The primers used were MP5 (5' ATTCATCCTTTTCA CACTAT 3') and the M13 universal sequencing primer (New England Biolabs). Diploid cells, generated from a cross of this marked strain with JBY007, were sporulated, and tetrads were dissected.

A chromosomal deletion of *VAC7* was created by a combination of PCR and homologous recombination (3). The *HIS3* gene was amplified by PCR. The first primer (V7OT) contained 43 bp of sequence from the 5' region of *VAC7* followed by 18 bp of the 3' end of *HIS3*. The second primer (V7OP) contained 43 bp of the *VAC7* 3' end and 18 bp to the *HIS3* 5' region. The primer sequences were 5' GCCACAATGCACGTCACTAATTCAAGAGAAATACCTTTTGCATTCGTTTCCAGATGACACG 3' (V7OT) and 5' ATCCTTTTGAATAGCCGT AGATTTTTCGCGTATTGAAAAAGGGCCCTCTTGGCCCTCCTCTAG 3' (V7OP). After PCR amplification, the product was transformed into the diploid wild-type yeast strain LWY6212 (LWY7221 \times LWY7224). Colony PCR was used to identify transformants that contained *HIS3* at the *VAC7* locus. The primers used were NL13 (5' TCACTCTGTGTTACTAAACGC 3') and His3 (5' TCATTATGTGATAATGCC 3'). The diploid was sporulated, and tetrads were dissected.

Construction of epitope-tagged Vac7p. The hemagglutinin A (HA) epitope-tagged *VAC7* was constructed as follows. The 2.4-kb *HindIII-HindIII* fragment encoding the amino-terminal region of Vac7p was subcloned into pUC19. Double-stranded mutagenesis (QuikChange kit; Stratagene) was used to introduce a *NotI* site between codons 330 and 331. To introduce the *NotI* site, the following primers were used in mutagenesis: 5' CGTAATGATGACACAGCGGCCG AAAAATATGCACTACATCT 3' and its complement, 5' AGATGTAGTCAT ATTTTGGCGCCGCTGGTGTATCATTACG 3'. A 100-bp *NotI-NotI* fragment that contained three tandem copies of HA from pGTEP (35) was inserted into the *NotI* site. Plasmids containing the HA fragment were sequenced (using fluorescent dye terminator automated sequencing) to ensure proper orientation of the insert. Plasmids with properly oriented inserts of 3, 6, and 12 HA tags were obtained. HA-*VAC7* fragments were subcloned into pCB3, a plasmid containing the full-length *VAC7*, to yield pCB26 (containing an internal 3-HA tag), pCB27 (containing an internal 6-HA tag), and pCB28 (containing an internal 12-HA tag). Internal HA-*VAC7*-containing plasmids were transformed into wild-type (RHY6210) and *vac7- Δ* 1 (LWY2045) strains.

Subcellular fractionations and Western blot analysis. Yeast strains were grown in synthetic medium at 24°C to an optical density at 600 nm (OD₆₀₀) of 1.5. Cells from 100 ml were harvested and washed once in 10 ml of ice-cold cytosol buffer (20 mM HEPES [pH 6.8], 0.15 M potassium acetate, 10 mM MgCl₂, and 0.25 M sorbitol). Cell pellets were resuspended in 1 ml of cytosol cocktail (cytosol buffer with the following protease inhibitors: 1 mg [each] of antipain, bestatin, pefabloc [Boehringer Mannheim], chymostatin, and E-64 [catalog no. E 3132; Sigma] per ml; 10 mM benzamide; 1 mM dithiothreitol; and 1 mM phenylmethylsulfonyl fluoride). Cells were transferred to a prechilled 15-ml Corax glass tube with 1.6 g of acid-washed glass beads. In a 4°C room, cells were vortexed vigorously for 30 s, followed by chilling on ice for 30 s; this cycle was repeated 10 times. The liquid was transferred to 1.5-ml tubes and centrifuged at 500 \times g at 4°C for 5 min to remove unbroken cells and cell wall debris.

Supernatant fractions were transferred to new tubes and centrifuged at 13,000 \times g at 4°C for 10 min. The resultant supernatant fractions (S13) were separated, and pellets (P13) were resuspended in 200 μ l of cytosol cocktail. S13 fractions were centrifuged at 100,000 \times g at 4°C for 1 h. Pellets (P100) also were resuspended in 200 μ l of cytosol cocktail. Laemmli sample loading buffer was added to equivalent OD units of each fraction. Samples were heated to 90°C for 5 min immediately prior to being loaded on a Laemmli (25) 7.5% polyacrylamide-sodium dodecyl sulfate (SDS) gel. After electrophoresis, proteins were transferred to nitrocellulose (ECL High Bond; Amersham) in Tris-glycine-methanol transfer buffer (46) at 30 V and 4°C for approximately 20 h. These long transfer times were used to ensure complete transfer of higher-molecular-mass proteins (monitored by observing the transfer of Rainbow protein ladder 220,000-Da molecular mass markers [Amersham Life Science]).

The standard Western blot protocol in the ECL manual (Amersham Life Science) was used, with monoclonal mouse anti-HA immunoglobulin G (IgG)

(MMSR101 [lot 7 175 1001]; BabCo) at a 1:1,000 dilution as the primary antibody. Goat anti-mouse IgG-horseradish peroxidase (Bio-Rad Laboratories, Hercules, Calif.) at a 1:2,000 dilution was employed as the secondary antibody. Bands were visualized with an ECL kit (Amersham Life Science) according to the manufacturer's instructions.

Extraction of Vac7p from the membrane. For the extraction of Vac7p from the membrane, crude cell extracts were prepared as described above. Prior to centrifugation, precleared cell extract was divided into six aliquots and treated under one of the following conditions: 2% Triton X-100, 1.4 M urea, 0.1 M Na₂CO₃ (pH 11.5), 1 M NaCl, 1 M hydroxylamine, or left untreated (buffer added to appropriate volume). Samples were allowed to incubate on ice for 20 min and then centrifuged at 150,000 \times g for 1 h at 4°C. The resultant supernatant fractions (S150) were separated, and pellets (P150) were resuspended in 100 μ l of cytosol cocktail. Equal amounts (as determined by ODs) were separated on an SDS-7.5% polyacrylamide gel, transferred to nitrocellulose, and probed as described above.

Treatment with PGNase. A P13 fraction was prepared as described above and resuspended in 50 μ l of cytosol cocktail. This was divided into two reaction mixtures, each with 20 μ l, and Triton X-100 was added to a final concentration of 1%. Samples were heated at 100°C for 2 min, and then the volume was brought up to 100 μ l by the addition of *N*-glycosidase F (PGNase) buffer (20 mM potassium phosphate [pH 7.2], 50 mM EDTA, and 0.5% Nonidet P-40). The reaction mixtures were heated again to 100°C for 2 min and allowed to cool to room temperature. Four units of PGNase (Boehringer Mannheim) was added to one tube, and the other tube was left untreated (buffer added). Reaction mixtures were incubated at 37°C, and 20- μ l aliquots were removed from each at the following time points: 1, 6, and 19 h. Twelve microliters of each sample was separated on an SDS-7.5% polyacrylamide gel, transferred to nitrocellulose, and probed as described above.

Stripping and reprobing with anti-100-kDa vacuolar ATPase subunit. Nitrocellulose blots prepared as described above were stripped by incubation in 100 mM 2-mercaptoethanol-2% SDS-62.5 mM Tris-HCl (pH 6.8) at 50°C for 30 min (ECL manual; Amersham Life Science). Membranes were rinsed twice in Tris-buffered saline-0.05% Tween 20 for 10 min at room temperature. The immunodetection protocol was repeated with monoclonal mouse anti-100-kDa vacuolar ATPase subunit IgG (Molecular Probes) at a 1:1,500 dilution. Nonfat dried milk (1.5%) in Tris-buffered saline-0.05% Tween 20 was used for dilutions of both antibodies.

Indirect immunofluorescence. (i) Localization of 60-kDa vacuolar ATPase. Log-phase cultures were used for indirect immunofluorescence as previously described (31). The primary antibody, mouse anti-60-kDa vacuolar ATPase subunit, was used at a 1:50 dilution (Molecular Probes), and the secondary antibody, a goat anti-mouse IgG conjugated with Oregon Green-488 (Molecular Probes), was used at a 1:240 dilution; each was incubated for 1 h.

(ii) Localization of HA-Vac7p. The indirect immunofluorescence protocol for anti-HA antibody (6) was carried out with a few modifications. Cells were suspended in sodium phosphate buffer (pH 6.5) and fixed by the addition of 37% formaldehyde to a final concentration of 4.4%. Fixation was carried out for 40 min with shaking at 30°C; this incubation time for the fixation step appears to be critical for preservation of the HA epitope for immunofluorescence (28a). Fixed cells were converted to spheroplasts by incubation in 1.2 M sorbitol in phosphate buffer (pH 6.5) with 1% 2-mercaptoethanol and 150 μ g of oxalyticase (Enzogenetics, Eugene, Oreg.) per ml for 10 to 15 min at 30°C. Ten microliters of washed spheroplasts was placed on 1% polyethyleneimine-coated multiwell slides (ICN Biomedicals, Aurora, Ohio) and allowed to attach by incubation for at least 30 min in a high-humidity chamber.

The blocking buffer and wash conditions of Berkower et al. (6) were used. Monoclonal mouse anti-HA IgG was used at a dilution of 1:200 and incubated overnight (~15 h). Oregon Green-488-conjugated goat anti-mouse IgG was used at a dilution of 1:240 for 1 h. For double-label immunofluorescence experiments, affinity-purified anti-Vac8p antibody, previously determined to localize to the vacuole membrane (48a), was used at a 1:50 dilution for 1 h of incubation. This was followed by rhodamine red-conjugated goat anti-rabbit IgG (a generous gift of Jackson ImmunoResearch Labs, Inc., West Grove, Pa.) at a 1:200 dilution. Images of labeled cells were collected by using an MRC 1024 scanning confocal head (BioRad Labs) mounted on a Nikon Optiphot equipped with a 100 \times oil immersion lens objective (1.4/NA).

For double immunofluorescence with anti-HA and anti-60-kDa ATPase, the protocol used for anti-HA immunofluorescence was carried out. Slides were incubated with monoclonal mouse anti-HA IgG at a 1:200 dilution for 15 h and then were incubated with the following antibodies in the order listed: goat anti-mouse IgG at a 1:300 dilution, rabbit anti-goat IgG at a 1:300 dilution, and Oregon Green-488-conjugated goat anti-rabbit IgG (Molecular Probes) at a 1:240 dilution. At this point, slides were incubated with mouse anti-60-kDa ATPase at a 1:50 dilution, followed by rhodamine lissamine-conjugated donkey anti-mouse IgG (Jackson ImmunoResearch Labs, Inc.) at a 1:200 dilution. Each incubation was performed for 1 h in a humidity chamber at room temperature. Intermediate washes were performed as described above. As negative controls, a series of incubations with the antibodies listed above was performed with either mouse anti-HA or mouse anti-60-kDa ATPase antibody omitted. Images were collected by confocal microscopy.

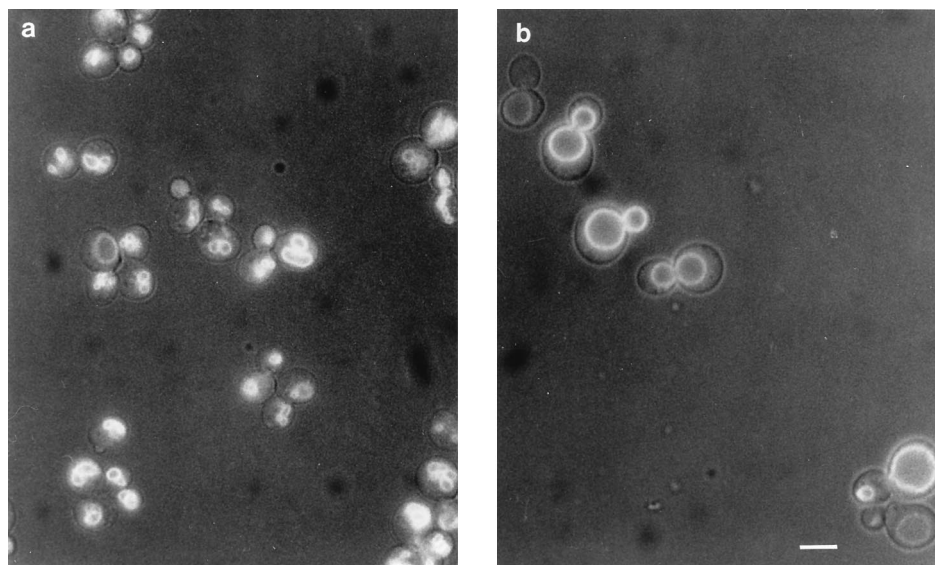






FIG. 1. *vac7-1* mutant exhibits both a vacuole inheritance defect and aberrant vacuole morphology. Wild-type (a) and *vac7-1* (b) vacuoles were labeled by adding 80 μ M FM4-64 to log-phase cultures at 24°C for 1 h. Labeled cells were washed twice in 1 ml of medium and allowed to grow in 5 ml of YEPD medium for 3 h (or one doubling) in a shaker at 24°C. Photographs were taken with a 100 \times objective lens on a Zeiss fluorescence microscope with an FT500/560 filter. Note that several *vac7-1* cells contain vacuoles between the mother and daughter cells with an open gap at the mother-daughter junction (open figure eight structure). Bar, 5 μ m.

RESULTS

The *vac7-1* strain is defective in vacuole inheritance and vacuole morphology. The *vac7-1* strain was identified by a plate assay designed to measure vacuole inheritance (15). The *vac7-1* strain has a vacuole inheritance defect, as measured both by fluorescence microscopy and by fluorescence-activated cell sorting (49); however, unlike most vacuole inheritance mutants, the *vac7* mutant also exhibits abnormal vacuole morphology. Wild-type cells usually contain a multilobed vacuole (Fig. 1a) and often contain segregation structures that extend from mother to daughter cells (53). In contrast, each *vac7-1* mutant cell contains a single swollen, unlobed vacuole (Fig. 1b). Moreover, 26% of *vac7-1* cells contain a vacuole that traverses the mother and daughter cells with a gap at the neck of the mother-daughter junction (termed an open figure eight) (Fig. 1 and Table 2). This structure appears to be a vacuole that fails to undergo membrane scission and form a separate vacuole in the daughter cell. In unsynchronized log-phase cultures, the fraction of *vac7-1* cells with this open figure eight is approximately equal to the observed number of wild-type cells with segregation structures (14).

The *vac7-1* mutant grows slowly in both rich liquid and solid

TABLE 2. Distribution of vacuole morphology in the *vac7-1* mutant

Strain ^a	% of cells with morphology			
				
RHY6210	100	0	0	0
<i>vac7-1</i>	0	58	26	16

^a Strains were labeled by adding 80 μ M FM4-64 to log-phase cultures at 24°C for 1 h. Labeled cells were washed in 1 ml of medium twice and chased in 5 ml of YEPD medium for one doubling at 24°C in a shaker. Five hundred cells of each strain were counted.

media at either 30 or 24°C. At 30°C in YEPD medium, the *vac7-1* strain has a doubling time of 2.5 h compared to 1.6 h for the parental strain (data not shown). The *vac7-1* strain also has a mild protein sorting defect. Carboxypeptidase Y (CPY) is processed slightly more slowly in this mutant than it is in the wild type, and less than 15% is missorted to the cell surface (15). This degree of CPY mislocalization is considerably lower than that of vacuole protein sorting (*vps*) mutants (31) and is similar to that reported for mutants with a vacuole acidification defect (23). The *vac7-1* strain also has a vacuole acidification defect (see below); thus, the mild vacuole protein sorting defect is most likely due to the acidification defect present in the *vac7-1* mutant.

One prominent defect of the *vac7-1* strain is its inability to undergo the vacuole membrane fission required to establish and maintain normal vacuole morphology and to allow vacuole segregation. We postulate that mutants of this type are defective in genes that are required for vacuolar scission; we have termed them class III mutants (49).

Other class III mutants. To date, we have identified three complementation groups that exhibit a vacuole membrane scission defect. In addition to the *vac7-1* mutant, the following two mutants display almost identical vacuole phenotypes (Fig. 2): the *fab1-2* mutant isolated by Yamamoto et al. (56) and the *vac14-1* mutant isolated via fluorescence-activated cell sorting in our laboratory. In the case of the *fab1-2* mutant, the vacuole morphology defects are present at 37°C but not at 24°C. *FAB1* encodes a large (257-kDa) polypeptide with homology to a mammalian type II phosphatidylinositol-4-phosphate 5-kinase, although the enzymatic activity of Fab1p remains to be demonstrated (56).

FAB1 expressed from a multicopy plasmid suppressed the vacuole morphology and vacuole inheritance defects of the *vac14-1* mutant (Fig. 3b), yet tetrad analysis demonstrated that *VAC14* was not allelic with *FAB1*. Of the 11 tetrads analyzed from a cross of *vac14* and *fab1* strains, nine tetratypes and two nonparental ditypes were obtained. The *vac14 fab1* double mutant is viable and has a phenotype similar to that of the

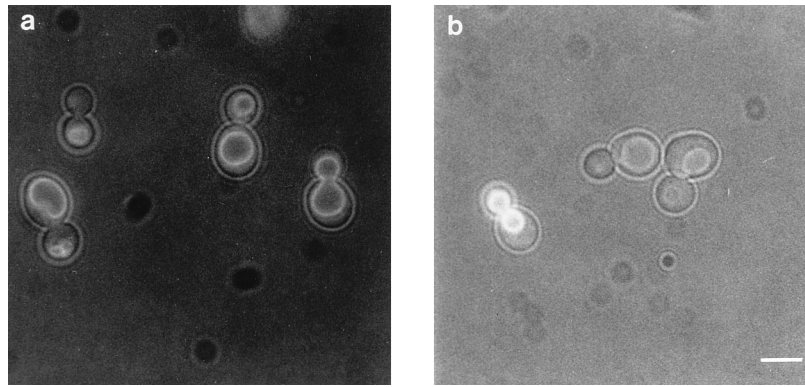


FIG. 2. Two other class III mutants exhibit almost identical vacuole morphologies. Vacuoles of the *fab1-2* (Ts) mutant (56) at the nonpermissive temperature (a) and the *vac14-1* mutant (b) were labeled with FM4-64 as described in the legend to Fig. 1. Bar, 5 μm .

vac14-1 mutant, further suggesting that *FAB1* and *VAC14* act in the same pathway.

Expression of *FAB1* either from a centromere-based plasmid or from a multicopy plasmid had no effect on *vac7-1* and *vac7- Δ 1* mutants. Likewise, there were no effects of *VAC7* expression from either centromere-based or multicopy plasmids on either the *vac14-1* or *fab1-2* mutant. However, we did detect some synthetic interactions between *vac7* and *fab1* and between *vac7* and *vac14*. *fab1-2 vac7-1* and *vac14-1 vac7-1* double mutants grew slower than did single mutants and also had significantly larger vacuoles. The *fab1-2* mutant had vacuoles of normal size and morphology at 24°C, whereas the diameter of vacuoles of the *fab1 vac7* strain were approximately $5.8 \pm 1.2 \mu\text{m}$ ($n = 50$) at 24°C, significantly larger than the diameter of *vac7-1* vacuoles ($4.1 \pm 0.9 \mu\text{m}$). The vacuole diameter of the *vac14 vac7* strain was $\sim 6.2 \pm 1.2 \mu\text{m}$, whereas the *vac14-1* vacuole diameter was $4.7 \pm 0.9 \mu\text{m}$.

The membrane scission defect is not due to enlarged vacuoles. One hypothesis that accounts for the vacuole morphology and inheritance defects of class III mutants is that the mutations indirectly produce a swollen vacuole through an accumulation of metabolites, degraded proteins, or ions in the vacuole. The large vacuole may prevent the vacuole membrane scission machinery from operating merely because the membranes are physically too far apart.

To test this possibility, wild-type cells were treated with either imidazole or rapamycin at 30°C. Vacuole morphology

and inheritance were examined after fluorescent labeling of vacuoles with FM4-64 (Fig. 4a and b). Imidazole, a weak base that can freely cross membranes, becomes trapped when it is protonated in the acidic environment of the vacuole. Although imidazole treatment did not swell the vacuoles to the same size as *vac7-1* vacuoles, wild-type vacuoles were enlarged but did not display the phenotypes associated with *vac7-1* vacuoles. Rapamycin, an immunophilin inhibitor, causes swelling of yeast vacuoles (7). We observed that yeast cells treated with rapamycin displayed normal vacuole inheritance, although vacuoles swelled to approximately the same size as *vac7* vacuoles (Fig. 4c) and the vacuoles of other class III mutants. Most notably, even when vacuoles were quite swollen, no open figure eight structures were seen. The vacuole diameter of rapamycin-treated cells, $4.2 \pm 0.8 \mu\text{m}$, was similar to the vacuole diameter of *vac7-1* cells, $4.1 \pm 0.9 \mu\text{m}$. This demonstrates that the membrane scission defect of class III mutants is not an indirect consequence of large vacuoles. Further, it supports the idea that membrane scission is not stochastic but requires specific molecules and that *VAC7*, *FAB1*, and *VAC14* function in this event.

To investigate whether *Vac7p* is directly involved in vacuole inheritance, a double mutant was created with *vac7-1* and *vps17*, a class B *vps* strain which contains highly vesiculated vacuoles (2), strains. The highly fragmented vacuoles of class B *vps* mutants may be due to the lack of a factor(s) that is required to maintain vacuolar structure (for a review, see reference 40); thus, this type of mutation may produce vesiculated vacuoles through a mechanism not related to *Vac7p*. The vacuoles of a *vac7 vps17* double mutant were fragmented and multilobed. Further, this double mutant did not display a vacuole inheritance defect (Fig. 4d). In addition, the double mutant missorted CPY (data not shown), as was shown for the *vps17* mutant (32), and had a defect in vacuole acidification (data not shown) similar to that in the *vac7-1* mutant.

The fragmented vacuoles in the double mutant may result from the introduction of hyperactive scission through the *vps17* mutation, causing the disappearance of unlobed vacuoles and open figure eight structures. The phenotype of the *vac7 vps17* strain suggests that the vacuole inheritance defect of class III mutants is secondary to the membrane scission defect. Thus, when vacuoles are fragmented due to the *vps17* mutation, the vacuole inheritance defect of the *vac7-1* mutant is suppressed. Moreover, it is unlikely that *vps17* represents a block at an early step of a linear pathway since the double mutant retains characteristics of each of the single mutants. In similar experiments, double mutants between the *fab1-2* mutant and a class

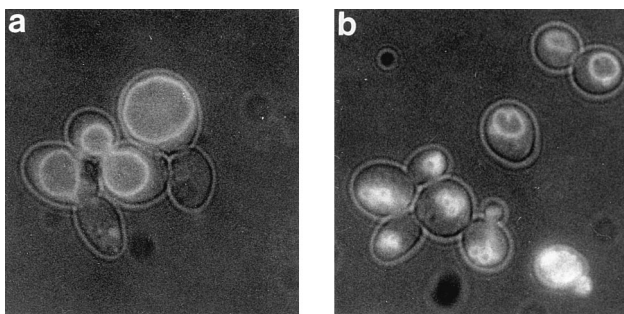


FIG. 3. *FAB1* suppresses the vacuole inheritance and morphology defects of the *vac14-1* mutant. Cells were stained with FM4-64 as described in Materials and Methods, washed with fresh medium, and allowed to double in fresh medium at 24°C. (a) The *vac14-1* mutant has a vacuole inheritance defect and large swollen vacuoles. (b) However, when the *vac14-1* mutant contains *FAB1* expressed on a multicopy plasmid, both vacuole morphology and vacuole inheritance defects are corrected.

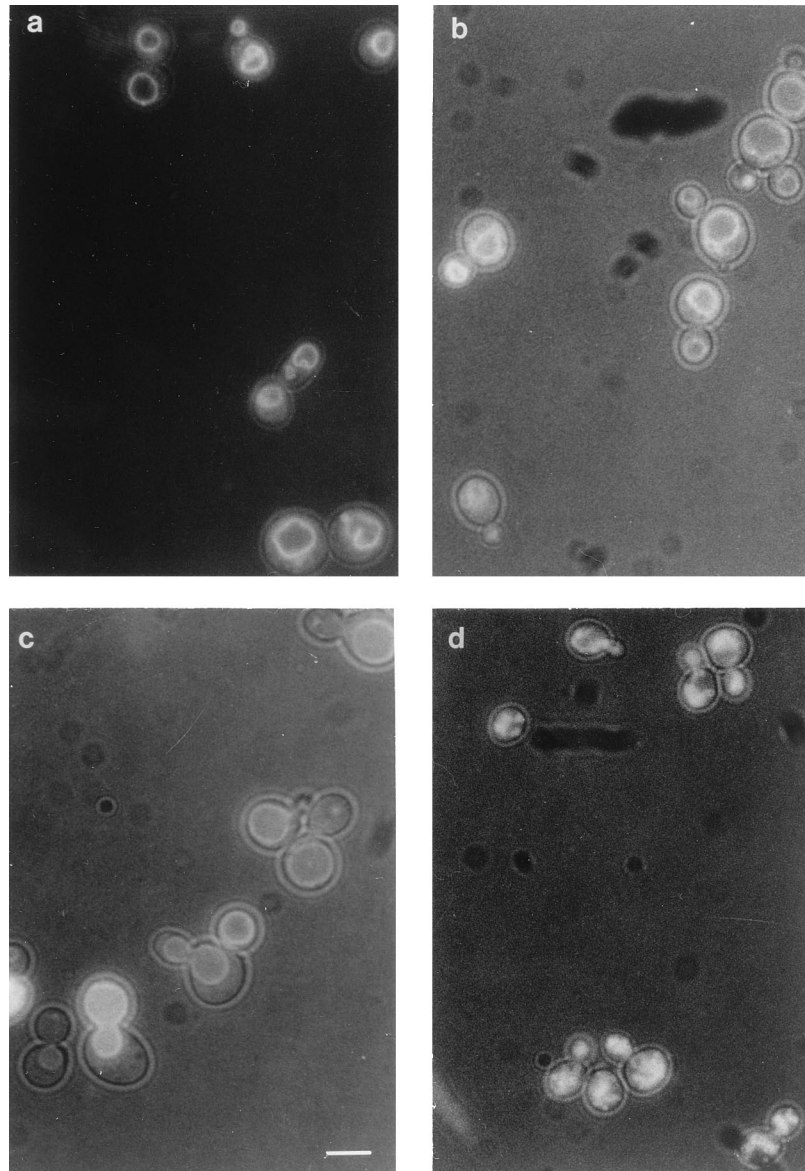


FIG. 4. Swelling vacuoles do not produce open figure eight structures or a vacuole inheritance defect. Wild-type yeast cells were incubated in 100 mM imidazole (a) or 0.8 μ g of rapamycin per ml (b), as described in Materials and Methods, and compared with untreated *vac7-1* cells (c). (d) Vacuole morphology of a *vac7 vps17* double mutant. To visualize vacuoles, all cells were labeled with 80 μ M FM4-64 for 1 h at 24°C, washed twice with fresh medium, and allowed to double in fresh medium at 24°C. Bar, 5 μ m.

C or E *vps* mutant were used to demonstrate that the aploid and binucleate phenotype of the *fab1* mutant was an indirect effect of vacuole size (56).

Vacuole membrane scission is not dynamin mediated. A BLASTp database search of the entire *S. cerevisiae*-translated open reading frames with shibire, the *Drosophila* dynamin homolog, and mouse dynamin protein sequences was performed. Two previously identified open reading frames, Dnm1p (12) and Vps1p (33), display global homology to dynamin and shibire. In addition, Mgm1p (16, 20) has high homology to a 159-amino-acid region, including the GTPase domain. Visualization of *dnm1- Δ 1*, *vps1*, and *mgm1- Δ 1* mutations by FM4-64 labeling clearly demonstrated that these mutations do not produce enlarged, unlobed vacuoles or the characteristic figure eight morphology which is characteristic of class III *vac* mutants (data not shown). This concurs with another study of the

dnm1- Δ 1 mutant, in which no vacuole membrane scission defect was observed (32a).

***vac7* and *vac14* mutants exhibit vacuole acidification defects.** While the wild-type vacuole pH is \sim 6.0, the vacuole pH of the *fab1-2* mutant is close to 7.0 (56). The other class III mutants, *vac7-1* and *vac14-1* strains, are also defective in vacuole acidification. Quinacrine, a fluorescent weak base, accumulates in the vacuole when it is protonated by the acidic environment, thus allowing visualization of wild-type vacuoles (51). *vac7-1* and *vac14-1* vacuoles were not labeled by quinacrine (Fig. 5b and c), indicating that their vacuoles were not acidified. This defect is not due to a mislocalized vacuolar ATPase. The 60-kDa subunit of the vacuolar ATPase appeared by indirect immunofluorescence to be properly localized to the vacuole membrane in *vac7-1* (49) and *vac14-1* and *fab1-2* (Fig. 6b and c) mutants. The assembly of the ATPase is subunit interde-

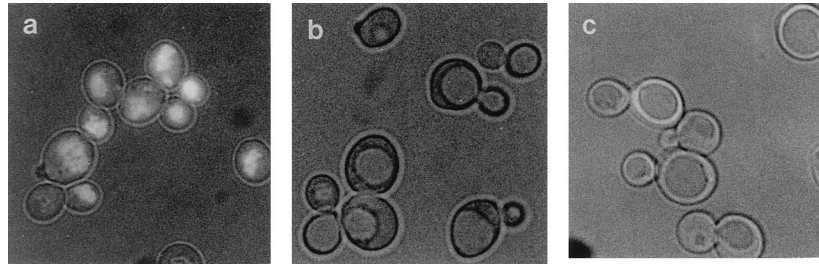


FIG. 5. *vac7-1* and *vac14-1* mutants have a vacuole acidification defect. Cells were labeled with 200 μ M quinacrine in potassium phosphate (pH 7.6)-buffered YEPD medium and washed twice in fresh medium. (a) Quinacrine staining is evident in the wild type, indicating normal vacuole acidification. (b and c) In both *vac7-1* and *vac14-1* mutants, respectively, vacuoles do not exhibit quinacrine fluorescence, which is indicative of the acidification defect. The photographs were taken by using both fluorescence and a low level of transmitted light.

pendent; when one subunit is lacking, the other subunits are not localized to the vacuolar membrane (22).

The vacuole acidification defect of the *vac14-1* mutant was suppressed by overexpression of wild-type *FAB1* from a centromere-based plasmid (Fig. 7d), even though the vacuole morphology was not corrected. *FAB1* expressed from a multi-copy plasmid also suppressed the vacuole acidification defect (Fig. 7c) and vacuole morphology defects in more than 90% of the population (Fig. 3b and 7c). Note that cells at the top of Fig. 7c contain multilobed vacuoles, whereas cells shown in the middle and bottom of this figure still exhibit single unlobed vacuoles, although they are considerably smaller than those in the original mutant. Although it is possible that vacuole acidification can be affected by increasing the volume of the vacuole, this is unlikely since the *vac7 vps17* mutant, which has highly vesiculated vacuoles, retains the acidification defect and the *vac14-1* mutant with low-copy *FAB1* has normal acidification but swollen vacuoles.

Cloning and sequencing *VAC7*. *VAC7* was cloned by complementation of a growth defect that the *vac7-1* mutant exhibits on high-pH, high-ethylene-glycol plates. This defect was not due to a general inability of the *vac7-1* strain to grow on nonfermentable carbon sources or high-osmolarity medium. The *vac7-1* mutant is able to grow on 1.0 M KCl, 1.5 M NaCl (data not shown), and ethanol-glycerol medium (15). Twelve clones that contained overlapping inserts and complemented both the growth defect and vacuolar morphology defect were isolated. A \sim 4.0-kb *Sna*BI-*Cla*I fragment was found to contain the single complementing open reading frame.

VAC7 was sequenced on both strands to reveal a 3.5-kb open reading frame, encoding a predicted protein of 1,165 amino acids. When the sequence of this region of chromosome XIV was first published by the Yeast Genome Sequencing Project,

there was an error in the middle of this open reading frame due to inversion of a cosmid (5). This has been corrected, and the open reading frame sequence has been deposited as YNL054W by the Yeast Genome Sequencing Project. There are no homologies with known proteins. The sequence is PEST rich throughout, contains an unusually high number of lysines and asparagines, and has runs of glutamines and aspartates. Computer analysis (PSORT and hydropathy plot analysis) revealed a potential transmembrane domain of approximately 24 amino acids in a region close to the carboxyl terminus between residues 919 and 943.

Chromosomal deletion of *VAC7*. A chromosomal deletion, *vac7- Δ 1*, was created by homologous recombination of *HIS3* flanked by *VAC7* sequence into the diploid strain LWY6212. Strains were checked for proper integration of *VAC7* flanked *HIS3* by colony PCR. The resulting diploid was sporulated, and 15 tetrads were dissected and analyzed. In each tetrad, *HIS3* cosegregated with the *vac7* phenotype. The chromosomal deletion was viable and had a vacuole phenotype similar to that of the *vac7-1* mutant; however, in the *vac7- Δ 1* mutant, vacuoles were more swollen and the growth rate decreased even further (data not shown). The difference in the severity of phenotypes suggests that the *vac7-1* allele retains partial function.

Localization of Vac7p. An HA-tagged *VAC7* was created by double-stranded mutagenesis and subcloning. The HA epitope was placed between amino acids 330 and 331, which are in a hydrophilic region of the Vac7p sequence. *VAC7* plasmids with 3, 6, and 12 tandem HA epitopes were obtained. All three plasmids complemented the *vac7- Δ 1* vacuole morphology and inheritance defects and had no effect on a wild-type strain, RHY6210 (data not shown). Indirect immunofluorescence showed that triple-HA-tagged Vac7p was localized to the vacuole membrane (Fig. 8a and b); it colocalized with a previously

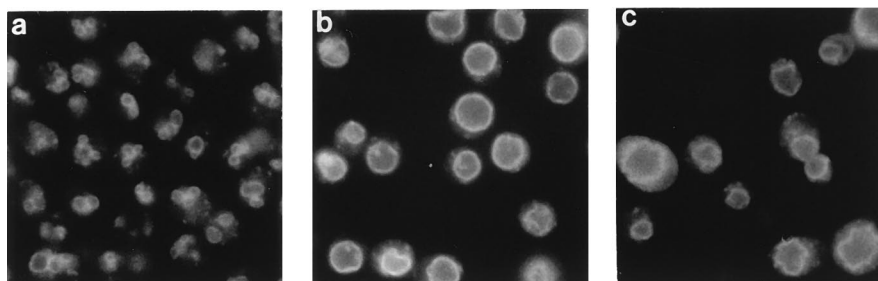


FIG. 6. Although *vac14-1* and *fab1-2* mutants display a vacuole acidification defect, the vacuolar ATPase is localized normally. Cells were grown at 24°C to log phase. *fab1-2* cells were shifted to 37°C for 2 h, whereas other cultures continued to be incubated at 24°C. Cells were fixed, converted to spheroplasts, and stained with monoclonal anti-60-kDa vacuolar ATPase at a 1:50 dilution. This subunit of the vacuolar ATPase was properly localized to the vacuole membrane in wild-type (a), *fab1-2* (at the nonpermissive temperature) (b), and *vac14-1* (c) cells.

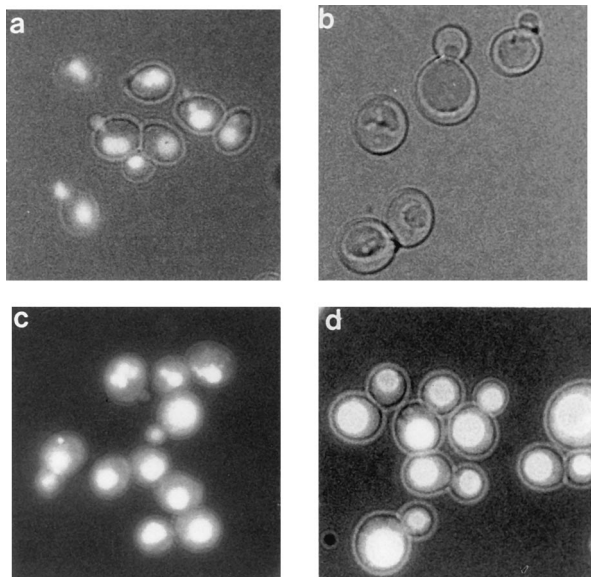


FIG. 7. Suppression of the acidification defect of the *vac14-1* mutant by *FABI*. Vacuolar acidification was monitored qualitatively by staining cells with quinacrine, a pH-sensitive vacuolar dye, as described in Materials and Methods. (a) Wild-type cells contain normally acidified vacuoles. The acidification defect of the *vac14-1* mutant (b) was corrected when the mutant contained *FABI* expressed on either a multicopy (c) or single-copy (d) plasmid. Note that *FABI* expressed on a single-copy plasmid corrected the acidification defect but not the vacuole morphology of the *vac14-1* mutant. The photographs were taken by using both fluorescence and a low level of transmitted light.

characterized vacuole membrane protein, Vac8p (48a). Similar results were obtained with 6- and 12-HA-tagged Vac7p in both the *vac7-Δ1* mutant and RHY6210 (data not shown). Three-HA-tagged Vac7p also localized to the vacuolar membrane in both the *vac14-1* mutant (Fig. 8c) and the *fab1-2* mutant at the nonpermissive temperature (Fig. 8d). Thus, the defects in *vac14* and *fab1* mutants are not due to mislocalization of Vac7p.

To confirm the localization of triple-HA-tagged Vac7p, double-label immunofluorescence was performed with antibodies to both HA and the 60-kDa subunit of the vacuolar ATPase (Fig. 9a and b). As both antibodies are mouse monoclonal IgGs, a complicated antibody sandwich was employed. We reasoned that if one of the mouse IgGs was buried by an antibody sandwich before the addition of the other mouse monoclonal antibody, cross-reactivity would be prevented. As controls, each of the primary antibodies was individually left out of the sandwich sequence (Fig. 9c through f).

Subcellular fractionation revealed triple-HA-tagged Vac7p in both a membrane-associated fraction that pelleted at $13,000 \times g$ (P13) and a fraction that pelleted only at $100,000 \times g$ (P100) (Fig. 10A). The immunoreactive polypeptide migrated to a molecular mass of approximately 150 kDa, which is slightly larger than the predicted size with three HA tags (132 kDa). The appearance of HA-tagged Vac7p in the P100 fraction may have been due to the method of cell breakage. It is likely that the use of glass beads resulted in breakage and vesiculation of a subset of vacuoles. The vacuole membrane was found predominantly in the P13 fraction; however, the presence of the 100-kDa subunit of the vacuolar ATPase in the P100 fraction (Fig. 10B) confirmed that this fraction also contained vacuolar membranes. Unfortunately, more gentle methods of breakage resulted in the appearance of considerably lower-molecular-weight forms of HA-tagged Vac7p in the sol-

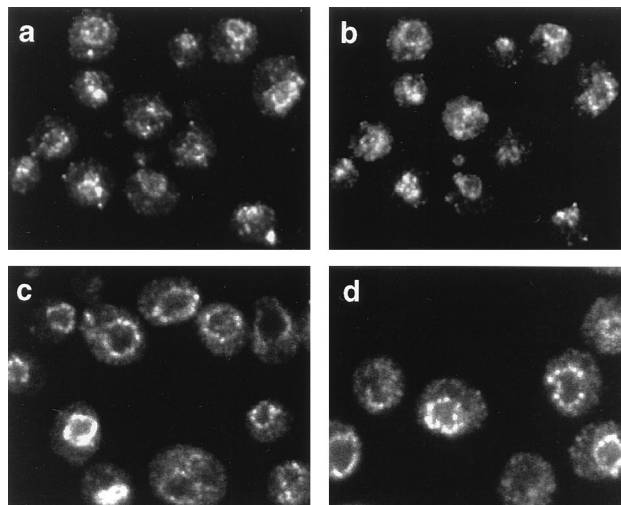


FIG. 8. Triple-HA-tagged Vac7p colocalizes with Vac8p, a vacuolar membrane protein. Cells were fixed in 4.4% formaldehyde for 40 min at 30°C. Fixed cells were converted to spheroplasts and incubated with monoclonal anti-HA (MMSR101; BabCo) at a 1:200 dilution overnight, followed by affinity-purified rabbit anti-Vac8p at a 1:50 dilution for 1 h. The primary mouse antibodies were detected by using Oregon Green-488-conjugated goat anti-mouse IgG (Molecular Probes), and rabbit antibodies were detected by Rhodamine Red-conjugated goat anti-rabbit IgG (Jackson ImmunoResearch Labs). Images were collected by using an MRC 1024 scanning confocal head mounted on a Nikon Optiphot equipped with a 100 \times oil immersion lens objective. Images were merged by using LaserSharp software and separated by using Corel Photo-Paint 7 software, and composites were made in Silicon Graphics by using Showcase 3.0 software. The two channels, green (a) and red (b), are shown separately, demonstrating that three-HA-tagged Vac7p (a) colocalized with Vac8p (b) at the vacuolar membrane. (c and d) *fab1-2* and *vac14-1* strains, respectively, harboring the Vac7-3XHA plasmid were incubated only with anti-HA antibody, followed by Oregon Green-488-conjugated goat anti-mouse IgG.

uble (S100) fraction. Most likely, this reflects the extreme susceptibility of a portion of HA-tagged Vac7p to proteolysis.

The sequence of *VAC7* reveals a putative transmembrane domain; therefore, to investigate whether Vac7p is a transmembrane protein or is peripherally associated, triple-HA-tagged Vac7p cell extracts were treated with various reagents (Fig. 10C). Only treatment with 2% Triton X-100 was able to solubilize Vac7p from the membrane; treatment with 1 M NaCl or 0.1 M carbonate (pH 11.5) did not extract Vac7p into the soluble fraction. This suggests that Vac7p is an integral membrane protein. The amino terminus of Vac7p has 16 putative glycosylation sites prior to the transmembrane domain, whereas the carboxy terminus has only 2 glycosylation sites. The treatment of triple-HA-tagged Vac7p cell extracts with PGNase did not noticeably alter the migration of triple-HA-tagged Vac7p on a 7.5% polyacrylamide-SDS gel; however, this treatment did deglycosylate CPY, resulting in a mobility shift (data not shown). This result is consistent with the large amino terminus being exposed to the cytoplasm, as the removal of core mannose oligosaccharides from 16 locations would have resulted in a visible mobility shift, whereas the removal of core mannose oligosaccharides from 2 locations would have changed the molecular mass of Vac7p by only approximately 5 kDa.

***vac7-1* defects are readily corrected in vivo during mating to wild-type yeast.** We monitored the effects of *vac7-1* on inter-vacuole exchange and vacuole morphology in heterozygous and homozygous zygotes. One of the parental haploids was labeled with FM4-64 and then mated to an unlabeled haploid. Vacuole morphology and FM4-64 transfer from the labeled

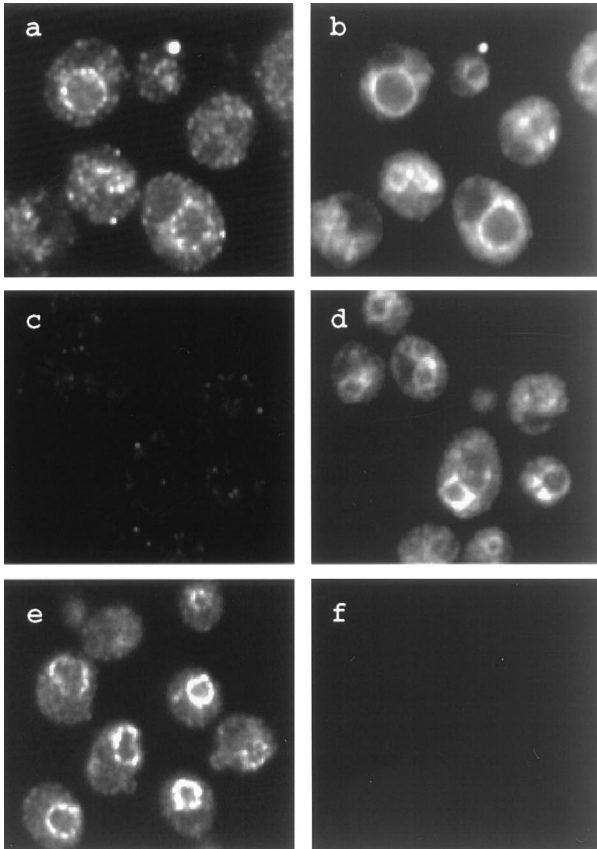


FIG. 9. Triple-HA-tagged Vac7p colocalizes with the 60-kDa subunit of the vacuolar ATPase. Cells were grown, fixed, and converted to spheroplasts as described in Materials and Methods. They were incubated with monoclonal anti-HA IgG at a 1:200 dilution for 15 h, followed by 1-h incubations with the following antibodies added sequentially in this order: goat anti-mouse IgG, rabbit anti-goat IgG, Oregon Green-488-conjugated goat anti-rabbit IgG, monoclonal anti-60-kDa subunit of the V-ATPase at a 1:50 dilution, and finally rhodamine lissamine-conjugated donkey anti-mouse IgG. Images were merged by using Laser sharp software and separated by using Corel Photo-Paint 7 software, and composites were made in Silicon Graphics by using Showcase 3.0 software. The two channels, green (a, c, and e) and red (b, d, and f), are shown separately. As controls, each primary antibody was omitted as follows: no anti-HA IgG antibody (c and d) and no anti-60-kDa subunit of the vacuolar ATPase antibody (e and f).

strain to the unlabeled parent through the bud was scored in zygotes with medium-to-large buds. Homozygous *vac7-ΔI/vac7-ΔI* zygotes could not be analyzed due to the lysis of a significant number of *vac7-ΔI* cells and thus the release of FM4-64 into the medium. In heterozygous zygotes, vacuole morphology was corrected quickly and FM4-64 transfer occurred normally (Table 3). In contrast, when *vac7-1* was mated with *vac7-ΔI*, the vacuoles in each cell remained single and unlobed and there was incomplete FM4-64 transfer to the unlabeled parent in ~60% of cells. This suggests that soluble components from the wild-type parent are able to correct the *vac7-1* defects. Zygotes had previously been used to demonstrate that vacuole segregation was not corrected in a *vac8/VAC8* heterozygote, despite the fact that *vac8-1* is a recessive allele (49). Vac8p is associated with the vacuole membrane (48a).

The results obtained with *vac7* zygotes, despite the vacuolar membrane localization of Vac7p (see above), can be accounted for as follows. First, Vac7p may produce or control the level of a soluble product or metabolite which, being freely diffusible,

enters the mutant parent and corrects the defects. Second, it is possible that wild-type Vac7p from the diploid nucleus is expressed in the zygote and rapidly recruited to the mutant vacuole.

DISCUSSION

The class III mutants, *vac7*, *vac14*, and *fab1* strains, share defects in vacuole morphology, vacuole acidification, and vacuole inheritance. These mutants may be primarily defective in molecules that are directly required for vacuole membrane scission. Particularly striking is the high percentage of cells in which the vacuole spans the mother and bud, with an open gap at the neck of the mother-bud junction (referred to as open figure eight structures). These vacuoles are unable to undergo membrane scission, with the result that the vacuole remains intact and spans the two cells. Similar structures are observed adjacent to the plasma membrane in a *shibire* strain, a *Drosophila* dynamin mutant (24). The defect in membrane scission in class III mutants also produces large, unlobed vacuoles. We have found that an enlarged vacuole alone is not sufficient to cause either the characteristic open figure eight structures or a vacuole inheritance defect. Despite these defects, vacuolar membrane fission can occur at a low rate in some class III *vac* mutant cells. This may be due to functionally redundant membrane scission machinery or occasional membrane fusion that occurs at a low frequency even in the absence of the normally required molecules. Cytokinesis may also force the completion of the vacuolar division by bringing the membranes close enough for scission to occur stochastically. Although the sequence of *VAC7* reveals no functional clues, Vac7p is an integral membrane protein that is localized at the vacuolar membrane. This places Vac7p at a position to act in vacuolar membrane scission either by direct involvement in membrane function or by regulating the molecules that are responsible for this specific membrane fusion.

In addition to the proteins required for scission, phospholipids play an important role. The phospholipid content of a particular membrane gives it distinct characteristics, such as curvature, rigidity, and permeability. Moreover, each type of cellular membrane has a distinct phospholipid composition. An indication that phospholipids play a critical role in vesicle formation came from the identification of Sec14p as a phospholipid transfer protein that is required to maintain an appropriate PC/PI ratio in the Golgi membrane (39). Furthermore, *in vitro* studies have determined that the phospholipid compositions of liposomes affect their fusogenicities (42, 43). Thus, the phospholipid content of the vacuolar membrane most likely influences its ability to undergo membrane scission.

Our class III mutants may represent genes that encode proteins which are involved in regulating the phospholipid composition of the vacuole membrane rather than proteins that function in a manner similar to that of dynamin or NSF. Fab1p most likely catalyzes the formation of phosphatidylinositol-4,5-phosphate [PtdIns(4,5)P] at the vacuole membrane (56). In addition, *vac14* displays genetic interactions with *FAB1*, suggesting that they function together. The acidification defect of the *vac14* mutant was suppressed by *FAB1* expressed from a low-copy plasmid, and the vacuole morphology defect of the *vac14* mutant was suppressed by *FAB1* expressed from a multicopy plasmid. We have continued to search for more complementation groups that exhibit a class III *vac* defect but have isolated only more alleles of *vac7*, *vac14*, and *fab1* (not shown). Thus, it is appealing to postulate that all three genes are related and are required for proper polyphosphoinositide content of the vacuole membrane.

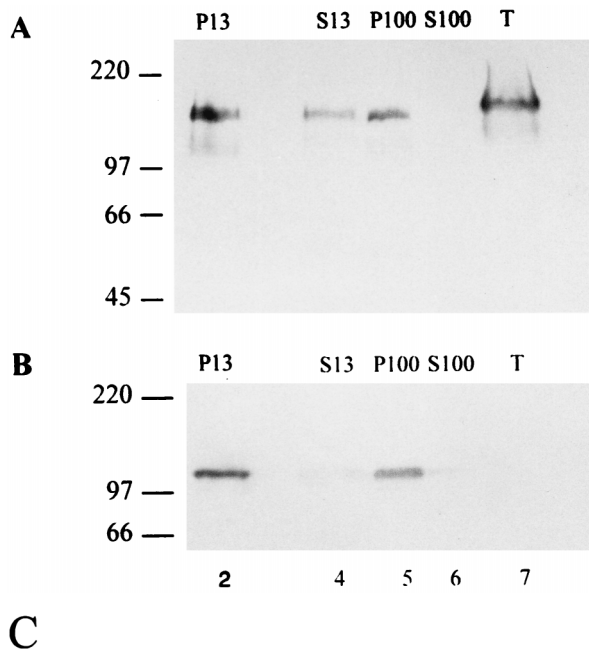
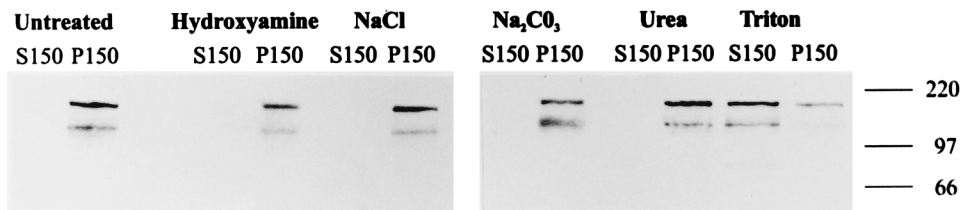


FIG. 10. Triple-HA-tagged Vac7p is associated with a membrane fraction. (A) Whole-cell extracts of cells containing the three-HA-tagged Vac7p were generated through glass bead breakage in cytosol cocktail containing 1 mM dithiothreitol and protease inhibitors. The crude extract was subjected to differential centrifugation. Equivalent amounts were loaded in all lanes. Lane 2, pellet resulting from $13,000 \times g$ spin (P13); lane 4, soluble fraction remaining after $13,000 \times g$ spin (S13); lane 5, pellet resulting from $100,000 \times g$ spin (P100); lane 6, soluble fraction remaining after $100,000 \times g$ spin (S100); lane 7, Total crude extract prior to centrifugation. The proteins were transferred to nitrocellulose, and Western blot analysis was performed. Molecular mass markers (in kilodaltons) are shown on the left. (B) The nitrocellulose membrane from panel A was stripped and reprobed with monoclonal anti-100-kDa ATPase (Molecular Probes) at a 1:1,500 dilution. The lane designations are the same as those for panel A. (C) Whole-cell extracts were prepared as described for panel A, divided into six equal aliquots, and treated on ice for 20 min under one of the following conditions: 2% Triton X-100, 1.4 M urea, 0.1 M Na_2CO_3 (pH 11.5), 1 M NaCl, 1 M hydroxyamine, or left untreated (buffer added to appropriate volume). Samples were centrifuged at $150,000 \times g$ for 1 h at 4°C . The resultant supernatant fractions (S150) were separated, and pellets (P150) were resuspended in 100 μl of cytosol cocktail. Equal amounts (as determined by ODs) were separated on an SDS-7.5% polyacrylamide gel, transferred to nitrocellulose, and probed with monoclonal anti-HA antibody (MMSR101; BabCo) at a 1:1,000 dilution.



Other evidence which suggests that vacuolar phospholipids are altered in class III mutants is the observation that although the vacuolar ATPase is localized correctly, the vacuoles in class III mutants are not properly acidified. There is no reason a priori for an inability to perform vacuole membrane scission to affect vacuole acidification. Yeast mutants that lack a subunit of the vacuolar ATPase and are defective in normal vacuole

acidification exhibit wild-type vacuole morphology and inheritance (not shown). The simplest explanation of how a single mutation can affect both vacuole membrane scission and acidification is a mutation that alters the vacuole membrane phospholipid composition. A change in membrane composition may disrupt the function of an ion channel or change the permeability of the membrane to protons. Alternatively, the ATPase may require a specific phospholipid (47), such as $\text{PtdIns}(4,5)\text{P}$ or a related metabolite, as a cofactor or to provide the necessary environment for function. Based on these data, *VAC7*, *VAC14*, and *FAB1* are more likely to be involved in a membrane function that is required for scission rather than acting enzymatically as scissors.

Yamamoto et al. proposed that the large vacuoles of the *fab1* mutant result from a defect in the efflux or turnover of the vacuole membrane and concluded that $\text{PtdIns}(4,5)\text{P}$ is essential for these processes. We have found that the vacuolar morphology and inheritance defects of the *fab1-2* mutant are very similar to those of the other class III mutants. The presence of open figure eight structures in the *fab1-2* strain suggests that it too is specifically defective in vacuole membrane scission, which may account for the defect in membrane turnover. Membrane efflux likely occurs through vesicle formation and thus requires scission. Given the genetic interaction between *FAB1* and *VAC14*, Vac14p may function as an activator of Fab1p; thus, when Fab1p is overexpressed, it bypasses the requirement for its activator. This is also consistent with the

TABLE 3. Quantification of vacuole morphology and inheritance in zygotes

Cross ^a	% of cells with morphology ^b			
	(None; <i>vac7</i>)	(To bud only; <i>vac7</i>)	(Normal; <i>vac7</i>)	(Normal; normal)
wt \times wt	0	0	0	100
<i>vac7</i> \times wt	0	1	4	95
<i>vac7</i> \times Δ<i>vac7</i>	21	45	33	1

^a Strains listed in bold were labeled with FM4-64 at 24°C for 1 h. Labeled cells were washed and chased in 5 ml of YEPD medium for 1 h. Then labeled cells were mixed with an equal amount of cells of the opposite mating type. Cultures were incubated at 24°C for 4 to 4.5 h. One hundred forty cells of each cross were counted. wt, wild type.

^b Parenthetical data refer to transfer from the labeled parent (top line) and vacuole morphology (bottom line).

viability and vacuolar phenotype of the *vac14 fab1* double mutant.

The functions of phospholipids, particularly PtdIns(4,5)P, in the fusion of vesicles with target organelles and in the membrane fusion that occurs with scission may be similar. Several potential roles of phospholipids, specifically PtdIns(4,5)P, in fusion can be envisioned. First, PtdIns(4,5)P may dock the necessary cytosolic proteins to the site of membrane scission or fusion (18, 29). A second potential role of phosphoinositides in membrane scission is through signaling. It has previously been demonstrated that Ca^{2+} mobilization through IP_3 receptors is required for nuclear fusion (41), in vitro liposome fusion (11), and the fusion of secretory granules with the plasma membrane (18). Moreover, Ca^{2+} is stored in the vacuole and IP_3 has previously been shown to stimulate its release (4). Third, the products of phospholipase D and phospholipase C may create a membrane section that is physically capable of undergoing membrane fusion by changing the phospholipid composition (18, 38). PtdIns(4,5)P is an activator of phospholipase D (27) and a substrate of phospholipase C. In artificial liposomes, increasing the phosphoinositol content decreases the fusogenicity, whereas phosphatidic acid increases fusogenicity (43). IP_3 production would also occur with the conversion of PtdIns(4,5)P to diacylglycerol and ultimately to phosphatidic acid, thus combining signal production with the change in membrane composition. The models discussed above are appealing because of the potential for tight control of the membrane fusion and fission events that are required to maintain organelle integrity and to coordinate membrane trafficking.

It is likely that class III mutants represent mutations in molecules that are essential for vacuole membrane scission. The location of Vac7p is consistent with this role. More detailed studies of the functions of class III *VAC* gene products and phospholipases D and C and of vacuolar Ca^{2+} levels will help to elucidate the molecular mechanisms involved.

ACKNOWLEDGMENTS

We thank Daniel Gomes de Mesquita and Conrad Woldringh for generously providing the *vac7-1* mutant prior to publication. We thank Scott Emr and Bill Snyder for providing us with *fab1-2* and *FAB1* on a multicopy plasmid and communicating unpublished results. We thank Joseph Heitman for discussions of rapamycin effects on vacuoles and for JK9-3D strains. We thank Janet Shaw for providing the *dnm1-Δ1* strain and for communicating her observations of this strain. We thank Aimee Kao and Emily Bristow for cloning the *VAC7* gene and Yuerong Zhu and Mark Pladett for their help with sequencing. We gratefully acknowledge Emily Bristow for excellent technical support. We thank Tom Monninger at the University of Iowa Central Microscopy Research Facility for help in using a confocal microscope and the University of Iowa DNA Core Facility for sequencing HA-*VAC7* plasmids. Finally, we thank Yong-Xu Wang, Kent Hill, Alice Fulton, and Robert Cohen for helpful discussions.

C. J. Bonangelino was supported by National Institute of General Medical Sciences NIH predoctoral grant 1 F31 GM18506-01. This work was also supported by a gift from the Roy J. Carver Charitable Trust to L. S. Weisman and National Institutes of Health grant GM50403.

REFERENCES

- Acharya, U., R. Jacobs, J.-M. Peters, N. Watson, M. G. Farquhar, and V. Malhotra. 1995. The formation of Golgi stacks from vesiculated Golgi membranes requires two distinct fusion events. *Cell* **82**:859–904.
- Banta, L. M., J. S. Robinson, D. J. Klionsky, and S. D. Emr. 1988. Organelle assembly in yeast: characterization of yeast mutants defective in vacuolar biogenesis and protein sorting. *J. Cell Biol.* **107**:1369–1383.
- Baudin, A., O. Ozier-Kalogeropoulos, A. Denouel, F. Lacroute, and C. Cullin. 1993. A simple and efficient method for direct gene deletion in *Saccharomyces cerevisiae*. *Nucleic Acids Res.* **21**:3329–3330.
- Belde, P. J. M., J. H. Vossen, G. H. F. H. Borst-Pauwels, and A. P. R.

- Theuvsnet. 1993. Inositol 1,4,5-triphosphate releases Ca^{2+} from vacuolar membrane vesicles of *Saccharomyces cerevisiae*. *FEBS Lett.* **323**:113–118.
- Bergez, P., F. Doignon, and M. Crouzet. 1995. The sequence of a 44,420 bp fragment located on the left arm of the chromosome XIV from *Saccharomyces cerevisiae*. *Yeast* **11**:967–974.
- Berkower, C., D. Loayza, and S. Michaelis. 1994. Metabolic instability and constitutive endocytosis of STE6, the α -factor transporter of *Saccharomyces cerevisiae*. *Mol. Biol. Cell* **5**:1185–1198.
- Cardenas, M. E., and J. Heitman. 1995. FKBP12-rapamycin target *TOR2* is a vacuolar protein with an associated phosphatidylinositol-4 kinase activity. *EMBO J.* **14**:5892–5907.
- Conibear, E., and T. H. Stevens. 1995. Vacuolar biogenesis in yeast: sorting out the sorting proteins. *Cell* **83**:513–516.
- Davis, R. W., M. Thomas, J. Cameron, T. P. St. John, S. Scherer, and R. A. Padgett. 1980. Rapid DNA isolation for enzymatic and hybridization analysis. *Methods Enzymol.* **65**:404–411.
- De Camilli, P. 1995. Molecular mechanisms in synaptic vesicle recycling. *FEBS Lett.* **369**:3–12.
- Duzgunes, N., J. Wilschut, R. Fraley, and D. Papahadjopoulos. 1981. Studies on the mechanism of fusion: role of head-group composition in calcium- and magnesium-induced fusion of mixed phospholipid vesicles. *Biochim. Biophys. Acta* **642**:182–195.
- Gammie, A. E., L. J. Kurihara, R. B. Vallee, and M. D. Rose. 1995. *DNM1*, a dynamin-related gene, participates in endosomal trafficking in yeast. *J. Cell Biol.* **130**:553–566.
- Gietz, R. D., A. Jean, R. A. Woods, and R. H. Schiestl. 1992. Improved method for high efficiency transformation of intact yeast cells. *Nucleic Acids Res.* **8**:1425.
- Gomes de Mesquita, D. S., R. ten Hoopen, and C. L. Woldringh. 1991. Vacuolar segregation to the bud of *S. cerevisiae*: an analysis of the morphology and timing in the cell cycle. *J. Gen. Microbiol.* **137**:2447–2454.
- Gomes de Mesquita, D. S., B. van den Haazel, J. Bouwman, and C. L. Woldringh. 1996. Characterization of new vacuolar segregation mutants, isolated by screening for loss of proteinase B self-activation. *Eur. J. Cell Biol.* **71**:237–247.
- Guan, K., L. Farh, T. K. Marshall, and R. J. Deschenes. 1993. Normal mitochondrial structure and genome maintenance in yeast requires the dynamin-like product of the *MGM1* gene. *Curr. Genet.* **24**:141–148.
- Haas, A., and W. Wickner. 1996. Homotypic vacuole fusion requires Sec17p (yeast alpha-SNAP) and Sec18p (yeast NSF). *EMBO J.* **15**:3296–3305.
- Hay, J. C., P. L. Fiset, G. H. Jenkins, K. Fukami, T. Takenawa, R. A. Anderson, and T. F. J. Martin. 1995. ATP-dependent inositide phosphorylation required for Ca^{2+} -activated secretion. *Nature* **374**:173–177.
- Heitman, J., N. R. Movva, and M. N. Hall. 1991. Targets for cell cycle arrest by the immunosuppressant rapamycin in yeast. *Science* **253**:905–909.
- Hill, K. L., N. L. Catlett, and L. S. Weisman. 1996. Actin and myosin function in directed vacuole movement during yeast cell division in *Saccharomyces cerevisiae*. *J. Cell Biol.* **135**:1535–1549.
- Jones, B. A., and W. L. Fangman. 1992. Mitochondrial DNA maintenance in yeast requires a protein containing a region related to the GTP-binding domain of dynamin. *Genes Dev.* **6**:380–389.
- Kaiser, C., S. Michaelis, and A. Mitchell. 1994. Methods in yeast genetics. Cold Spring Harbor Laboratory Press, Cold Spring Harbor, N.Y.
- Kane, P. M., M. C. Kuehn, I. Howald-Stevenson, and T. H. Stevens. 1992. Assembly and targeting of peripheral and integral membrane subunits of the yeast vacuolar H^+ -ATPase. *J. Biol. Chem.* **267**:447–454.
- Klionsky, D. J., H. Nelson, and N. Nelson. 1992. Compartment acidification is required for efficient sorting of proteins to the vacuole in *Saccharomyces cerevisiae*. *J. Biol. Chem.* **267**:3416–3422.
- Koenig, J. H., and K. Ikeda. 1989. Disappearance and reformation of synaptic vesicle membrane upon transmitter release observed under reversible blockage of membrane retrieval. *J. Neurosci.* **9**:3844–3860.
- Laemmli, U. K. 1970. Cleavage of structural proteins during the assembly of the head of bacteriophage T4. *Nature* **227**:680–685.
- Latterich, M., K.-U. Frohlich, and R. Schekman. 1995. Membrane fusion and the cell cycle: Cdc48p participates in the fusion of ER membranes. *Cell* **82**:885–893.
- Liscovitch, M., V. Chalifa, P. Pertile, C.-S. Chen, and L. C. Cantley. 1994. Novel function of phosphatidylinositol 4,5-bisphosphate as a cofactor for brain membrane phospholipase D. *J. Biol. Chem.* **269**:21403–21406.
- Mellman, I. 1994. Membranes and sorting. *Curr. Opin. Cell Biol.* **6**:497–498.
- Michaelis, S. (Johns Hopkins University). Personal communication.
- Ohashi, M., K. Jan de Vries, R. Frank, G. Snoek, V. Bankaitis, K. Wirtz, and W. B. Huttner. 1995. A role for phosphatidylinositol transfer protein in secretory vesicle formation. *Nature* **377**:544–547.
- Rabouille, C., T. P. Levine, J.-M. Peters, and G. Warren. 1995. An NSF-like ATPase, p97, and NSF mediate cis-ternal regrowth from mitotic Golgi fragments. *Cell* **82**:905–914.
- Raymond, C. K., I. Howald-Stevenson, C. A. Vater, and T. H. Stevens. 1992. Morphological classification of the yeast vacuolar protein sorting mutants: evidence for a prevacuolar compartment in class E *vps* mutants. *Mol. Biol. Cell* **3**:1389–1402.

32. **Robinson, J. S., D. J. Klionsky, L. M. Banta, and S. D. Emr.** 1988. Protein sorting in *Saccharomyces cerevisiae*: isolation of mutants defective in the delivery and processing of multiple vacuolar hydrolases. *Mol. Cell. Biol.* **8**:4936–4948.
- 32a. **Roeder, A. D., D. Otsuga, and J. M. Shaw (University of Utah).** Personal communication.
33. **Rothman, J. E., C. K. Raymond, T. Gilbert, P. J. O'Hara, and T. H. Stevens.** 1990. A putative GTP binding protein homologous to interferon-inducible Mx proteins performs an essential function in yeast protein sorting. *Cell* **61**:1063–1074.
34. **Rothman, J. E., and F. T. Wieland.** 1996. Protein sorting by transport vesicles. *Science* **272**:227–234.
35. **Schneider, B. L., W. Seufert, B. Steiner, Q. H. Yang, and A. B. Futcher.** 1995. Use of polymerase chain reaction epitope tagging for protein tagging in *Saccharomyces cerevisiae*. *Yeast* **11**:1265–1274.
36. **Sears, L. E., L. S. Moran, C. Kissinger, T. Creasey, H. Perry-O'Keefe, M. Roskey, E. Sutherland, and B. S. Slatko.** 1992. Circum Vent thermal cycle sequencing and alternative manual and automated DNA sequencing protocols using highly thermostable Vent_R (exo-) DNA polymerase. *BioTechniques* **13**:626–633.
37. **Sikorski, R. S., and P. Hieter.** 1989. A system of shuttle vectors and yeast host strains designed for efficient manipulation of DNA in *Saccharomyces cerevisiae*. *Genetics* **122**:19–27.
38. **Simon, J., I. E. Ivanov, M. Adesnik, and D. D. Sabatini.** 1996. The production of post-Golgi vesicles requires a protein kinase C-like molecule, but not its phosphorylating activity. *J. Cell Biol.* **135**:355–370.
39. **Skinner, H. B., T. P. McGee, C. R. McMaster, M. R. Fry, R. M. Bell, and V. A. Bankaitis.** 1995. The *Saccharomyces cerevisiae* phosphatidylinositol-transfer protein effects a ligand-dependent inhibition of choline-phosphate cytidyltransferase activity. *Proc. Natl. Acad. Sci. USA* **92**:112–116.
40. **Stack, J. H., B. Horazdovsky, and S. D. Emr.** 1995. Receptor-mediated protein sorting to the vacuole in yeast: roles for a protein kinase, a lipid kinase and GTP-binding proteins. *Annu. Rev. Cell Dev. Biol.* **11**:1–33.
41. **Sullivan, K. M. C., W. B. Busa, and K. L. Wilson.** 1993. Calcium mobilization is required for nuclear vesicle fusion in vitro: implications for membrane traffic and IP₃ receptor function. *Cell* **73**:1411–1422.
42. **Sundler, R., N. Duzgunes, and D. Papahadjopoulos.** 1981. Control of membrane fusion by phospholipid head groups. The role of phosphatidylethanolamine in mixtures with phosphatidate and phosphatidylinositol. *Biochim. Biophys. Acta* **649**:751–758.
43. **Sundler, R., and D. Papahadjopoulos.** 1981. Control of membrane fusion by phospholipid head groups. Phosphatidate/phosphatidylinositol specificity. *Biochim. Biophys. Acta* **649**:743–750.
44. **Takei, K., P. S. McPherson, S. L. Schmid, and P. De Camilli.** 1995. Tubular membrane invaginations coated by dynamin rings are induced by GTP-γS in nerve terminals. *Nature* **374**:186–190.
45. **Takei, K., O. Mundigl, L. Daniell, and P. De Camilli.** 1996. The synaptic vesicle cycle: a single vesicle budding step involving clathrin and dynamin. *J. Cell Biol.* **133**:1237–1250.
46. **Towbin, H., T. Staehelin, and J. Gordon.** 1979. Electrophoretic transfer of proteins from polyacrylamide gels to nitrocellulose sheets: procedure and some applications. *Proc. Natl. Acad. Sci. USA* **76**:4350–4354.
47. **Uchida, E., Y. Ohsumi, and Y. Anraku.** 1988. Purification of yeast vacuolar membrane H⁺-ATPase and enzymological discrimination of three ATP-driven proton pumps in *Saccharomyces cerevisiae*. *Methods Enzymol.* **157**:544–563.
48. **Vida, T. A., and S. D. Emr.** 1995. A new vital stain for visualizing vacuolar membrane dynamics and endocytosis in yeast. *J. Cell Biol.* **128**:779–792.
- 48a. **Wang, Y.-X., N. L. Catlett, and L. S. Weisman.** Submitted for publication.
49. **Wang, Y.-X., H. Zhao, T. Harding, D. S. Gomes de Mesquita, C. L. Woldring, D. J. Klionsky, A. L. Munn, and L. S. Weisman.** 1996. Multiple classes of yeast mutants are defective in vacuole partitioning yet target vacuole proteins correctly. *Mol. Biol. Cell* **7**:1375–1389.
50. **Warren, G., and W. Wickner.** 1996. Organelle inheritance. *Cell* **84**:395–400.
51. **Weisman, L. S., R. Bacallao, and W. Wickner.** 1987. Multiple methods of visualizing the yeast vacuole permit evaluation of its morphology and inheritance during the cell cycle. *J. Cell Biol.* **105**:1539–1547.
52. **Weisman L. S., S. D. Emr, and W. Wickner.** 1990. Mutants of *Saccharomyces cerevisiae* that block intervacuole vesicular traffic and vacuole division and segregation. *Proc. Natl. Acad. Sci. USA* **87**:1067–1080.
53. **Weisman, L. S., and W. Wickner.** 1988. Intervacuole exchange in the yeast zygote: a new pathway in organelle communication. *Science* **241**:589–591.
54. **Weisman, L. S., and W. Wickner.** 1992. Molecular characterization of *VAC1*, a gene required for vacuole inheritance and vacuole protein sorting. *J. Cell Biol.* **267**:618–623.
55. **Xu, Z., A. Mayer, E. Muller, and W. Wickner.** 1997. A heterodimer of thioredoxin and IB₂ cooperates with Sec18p (NSF) to promote yeast vacuole inheritance. *J. Cell Biol.* **136**:299–306.
56. **Yamamoto, A., D. B. DeWald, I. V. Boronenkov, R. A. Anderson, S. D. Emr, and D. Koshland.** 1995. Novel PI(4)P 5-kinase homologue, Fab1p, essential for normal vacuole function and morphology in yeast. *Mol. Biol. Cell* **6**:525–539.